The EMBO Journal (2005) 24, 3224–3234 | © 2005 European Molecular Biology Organization | All Rights Reserved 0261-4189/05
www.embojournal.org

THE EMBO JOURNAL

Conformational changes of pore helix coupled to gating of TRPV5 by protons

Byung-Il Yeh[1,2], Yung Kyu Kim[1], Wasey Jabbar[1] and Chou-Long Huang[1,2,*]

[1]Department of Medicine, University of Texas Southwestern Medical Center, Dallas, TX, USA and [2]Charles & Jane Pak Center for Mineral Metabolism and Clinical Research, University of Texas Southwestern Medical Center, Dallas, TX, USA

The transient receptor potential channel TRPV5 constitutes the apical entry pathway for transepithelial Ca^{2+} transport. We showed that TRPV5 was inhibited by both physiological intra- and extracellular acid pH. Inhibition of TRPV5 by internal protons was enhanced by extracellular acidification. Similarly, inhibition by external protons was enhanced by intracellular acidification. Mutation of either an extra- or an intracellular pH sensor blunted the crossinhibition by internal and external protons. Both internal and external protons regulated the selectivity filter gate. Using the substituted cysteine accessibility method, we found that intracellular acidification of TRPV5 caused a conformational change of the pore helix consistent with clockwise rotation along its long axis. Thus, rotation of pore helix caused by internal protons facilitates closing of TRPV5 by external protons. This regulation by protons likely contributes to pathogenesis of disturbances of Ca^{2+} transport in many diseased states. Rotation of pore helix may be a common mechanism for crossregulation of ion channels by extra- and intracellular signals.

The EMBO Journal (2005) **24,** 3224–3234. doi:10.1038/sj.emboj.7600795; Published online 25 August 2005
Subject Categories: membranes & transport
Keywords: substituted cysteine-accessibility method; transepithelial Ca^{2+} transport; transient receptor potential

Introduction

Transient receptor potential (TRP) channels are widespread and play many important functions, ranging from store- and receptor-operated Ca^{2+} entry, thermal, tactile, taste, osmolar, and fluid flow sensing, embryonic development to epithelial Ca^{2+} and Mg^{2+} transport (Hoenderop *et al*, 2002; Montell *et al*, 2002; Clapham, 2003; Huang, 2004). TRP channels are classified into TRPC, TRPV, TRPM TRPP, TRPML, TRPN, and TRPA subfamilies. The TRPV subfamily is named after the first mammalian member of the subfamily, vanilloid receptor 1 (VR1), and contains six mammalian members, TRPV1–6 (Jordt *et al*, 2003). TRPV5 and TRPV6 are the only two highly Ca^{2+}-selective TRP channels and mediate *trans*-epithelial Ca^{2+} transport in the kidney and intestine (Hoenderop *et al*, 2002). Structurally, all TRP channels have six predicted transmembrane (TM) segments and N- and C-terminal cytoplasmic tails similar to the topologies of voltage-gated K^+, Na^+, and Ca^{2+} channels, cyclic nucleotide-gated (CNG) channels, and hyperpolarization-activated channels (Montell *et al*, 2002; Clapham, 2003). The six-TM polypeptide subunits of TRP channels likely assemble as tetramers to form cation-permeable pores (Hoenderop *et al*, 2003).

The bacterial K^+ channel KcsA contains two membrane-spanning segments and an intervening pore (P) loop (Doyle *et al*, 1998). The crystal structure of KcsA reveals an outer selectivity filter gate stabilized by pore helices and an inner gate formed by four inner helices of four identical subunits packed against each other as a bundle near the intracellular aspect of the membrane, giving an appearance of an inverted teepee (Doyle *et al*, 1998). This architecture is likely a general structure for all P-loop-containing channels including voltage-gated K^+ channels, inward rectifier and Ca^{2+}-activated K^+ channels, and CNG cation channels (Flynn *et al*, 2001). How and which gate is activated by individual extra- and intracellular signals for each channel is under intense investigation. The location of the inner gate suggests its role as an activation gate for intracellular signals. However, signals acting from the intracellular aspect of the membrane also impact on the selectivity filter (Flynn and Zagotta, 2001).

TRPV5 is localized to the apical membrane of polarized epithelia and functions as a gatekeeper for transepithelial Ca^{2+} transport (Hoenderop *et al*, 2002). Transepithelial Ca^{2+} transport is inhibited in conditions associated with overproduction of acids (Sutton *et al*, 1979). How acid inhibits transepithelial Ca^{2+} transport is not known. One potential mechanism is by direct inhibition of the TRPV5 channel. Little is known about the structure and mechanism involved in the gating of TRP channels. Mutation of aspartate-542 of TRPV5 greatly reduces Ca^{2+} permeation, indicating that the aspartate and adjacent amino acids form the selectivity filter in the channel (Nilius *et al*, 2001). A stretch of ~20 amino acids in the pre-selectivity filter region of TRPV5 and TRPV6 is highly homologous to that in KcsA and cysteine-substituted mutants of the region exhibit a cyclic pattern of reactivity to MTS reagents (Dodier *et al*, 2004; Voets *et al*, 2004). Thus, this region likely forms the pore helix of TRPV5 and TRPV6.

In this study, we show that the selectivity filter gate of TRPV5 is crossregulated by physiological extra- and intracellular pH (pH_i). Gating of TRPV5 by intracellular acidification is coupled with a clockwise rotation of the pore helix. This intracellular proton-induced conformational change of the pore helix facilitates gating by extracellular protons. These results provide a novel mechanism for crossregulation of ion channels by intra- and extracellular signals.

*Corresponding author. Department of Medicine, University of Texas Southwestern Medical Center, Room J5-104A, MC-8856, 5323 Harry Hines Blvd, Dallas, TX 75390-8856, USA. Tel.: +1 214 648 8627; Fax: +1 214 648 2071; E-mail: chou-long.huang@utsouthwestern.edu

Received: 1 September 2004; accepted: 2 August 2005; published online: 25 August 2005

Results

Inhibition of TRPV5 by intracellular acidification

We examined pH_i regulation of TRPV5 by inside-out patch-clamp recording (Figure 1A). As shown, TRPV5 currents were recorded using voltage ramps (from −100 to 100 mV over 400 ms). In inside-out patches, TRPV5 exhibited inwardly rectifying currents in divalent-free (DVF) cytoplasmic solutions (see Figure 1B ramp *I–V* curve at pH_i 9.0: outward (at 100 mV) and inward currents (at −100 mV) were 197 and −412 pA, respectively). The Mg^{2+}-independent inward rectification has been suggested due to intrinsic gating (Voets *et al*, 2003). Maximal TRPV5 currents occurred when inside-out membranes were exposed to solutions with pH 9.0–9.5 (Figure 1B and C). Decreasing pH from 9.0 to 4.9 caused a progressive reduction of TRPV5 currents, which reversed upon increasing the pH to 9.0 (Figure 1C). At an extracellular pH (pH_e) of 7.2 (illustrated in Figure 1A), the apparent pK_a for pH_i regulation was estimated at 7.31 ± 0.12 ($n = 21$) (Figure 1D). The *Hill* coefficient for pH_i regulation is ~2.1, indicating that each channel is gated by more than one proton and with cooperativity. Thus, TRPV5 is steeply gated by internal protons at physiological and pathophysiological pH_i's.

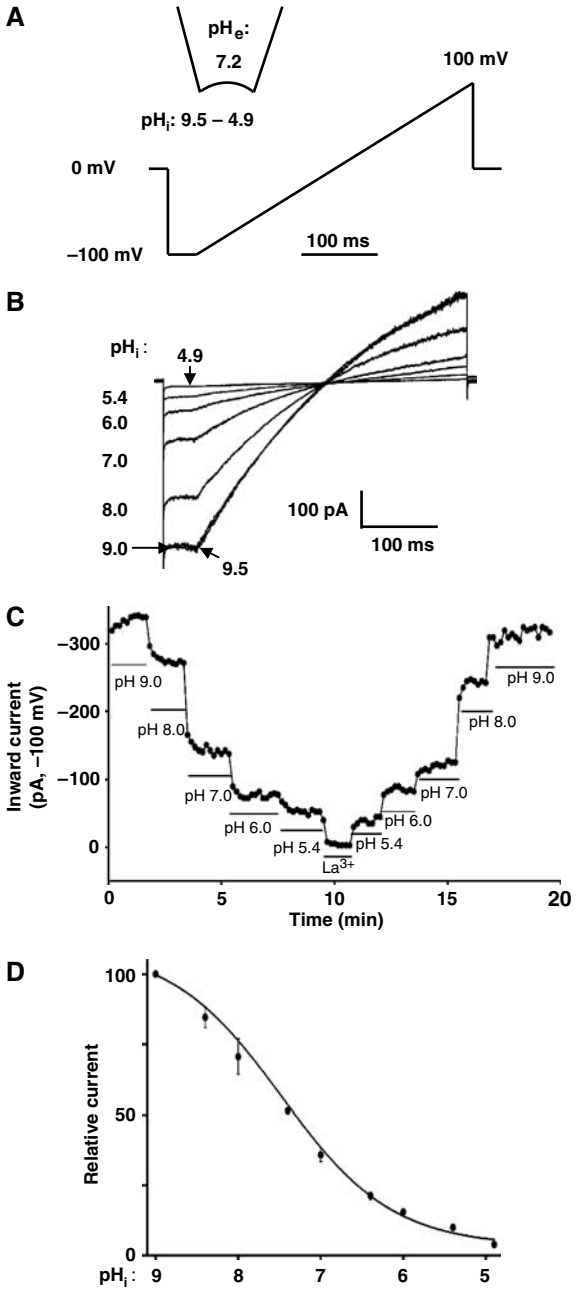

Figure 1 Regulation of TRPV5 by pH_i and its modulation by pH_e. (**A**) Inside-out recording and voltage ramp protocol (applied every 10 s). (**B**) Current–voltage (*I–V*) relationships of currents (in DVF solution) at different pH_i's. The degree of inward rectification in our study appears to be slightly less than that in some study (Voets *et al*, 2003). Mechanism(s) for the apparent difference awaits further study. (**C**) Inward currents (pA, at −100 mV) at different pH_i's over time. Currents through TRPV5 were inhibited by lanthanum (La^{3+}, 10 mM). In mock-transfected cells, increasing pH_i from 4.9 to 9.4 caused a relatively insignificant increase of background inward currents (<50 pA, compared to the mean maximal inward TRPV5 currents at pH_i 9.4 (452 ± 18 pA, $n = 21$)). (**D**) Dose–response curve for inhibition of TRPV5 by intracellular acid. Relative currents (after subtraction of residual currents in 10 mM La^{3+}, normalized to the maximal current, labeled as 100) at any given pH_i are shown.

Effects of internal protons on TRPV5 single-channel properties were further studied. As shown in the representative recording with only one active channel in the patch, single-channel open probability (P_o) was higher at pH_i 8.4 than at 7.0 (P_o: 0.86 versus 0.24; Supplementary Figure 1A). In multiple recordings, the average NP_o (number of channels in the excised patch $[N] \times P_o$) at pH_i's 8.4 and 7.0 were 3.05 ± 1.1 and 0.97 ± 0.4, respectively ($P < 0.05$; Supplementary Figure 1B). Single-channel conductance (measured between −25 and −75 mV) at pH_i's 8.4 and 7.0 were 78.2 ± 4.6 and 60.4 ± 2.6 pS, respectively ($P < 0.05$; Supplementary Figure 1C). Thus, as for external protons (Yeh *et al*, 2003), intracellular protons reduce single-channel conductance as well as open probability.

Modulation of pH_i regulation of TRPV5 by pH_e

Extracellular protons also inhibit TRPV5 (Yeh *et al*, 2003). We investigated the potential modulation by pH_e of pH_i regulation of TRPV5. Effects of pH_i on TRPV5 at various extracellular (pipette) pH's were studied using inside-out recordings (Figure 2A). Increasing the pH_e from 7.2 (indicated by the open triangle curve in Figure 2A and second bar from right in Figure 2B) to 8.4 (black curve and black bar in Figure 2) caused a shift in the pK_a for pH_i regulation toward more acidic values (see Supplementary Figure 2A and B for original traces). Conversely, decreasing pH_e from 7.2 to 6.8 caused a shift in pK_a for pH_i regulation toward more alkaline pH (Figure 2A and B; Supplementary Figure 2C and D). Thus, opening and closing of the channel by extracellular alkalinization and acidification, respectively, facilitates opening and closing by intracellular alkalinization and acidification. Intra- and pH_e could crossregulate TRPV5 by acting on the same gate or by regulating different activation gates. The pH_e-induced shift in pK_a for pH_i regulation based on normalized relative current, nevertheless, suggests that both pH's cross-regulate the same gate.

Modulation of pH_e regulation of TRPV5 by pH_i

If both pH's regulate the same gate, pH_i would also modulate pH_e regulation of the channel. Using whole-cell recordings (Figure 3A), decreasing intracellular (pipette) pH's from 8.4 to 6.4 caused a shift in pK_a for pH_e regulation from 5.1 ± 0.1 to 7.3 ± 0.1 (Figure 3A and B), indicating that intracellular

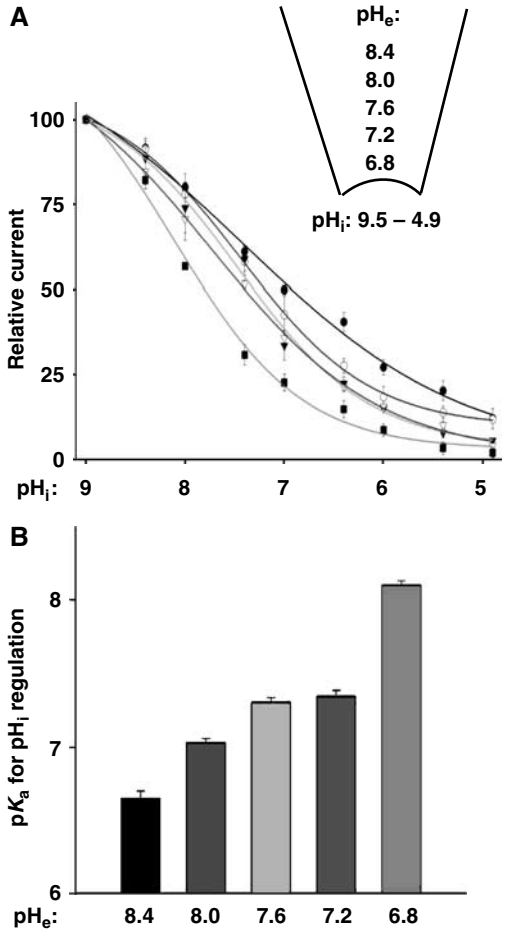

Figure 2 Modulation of pH_i regulation of TRPV5 by pH_e. (**A**) Dose–response curves for pH_i regulation (pH_i from 9.5 to 4.9) at different pH_e's. Experimental paradigm is as in Figure 1D. (**B**) pK_a for pH_i regulation (*Y*-axis) at different pH_e's (*X*-axis).

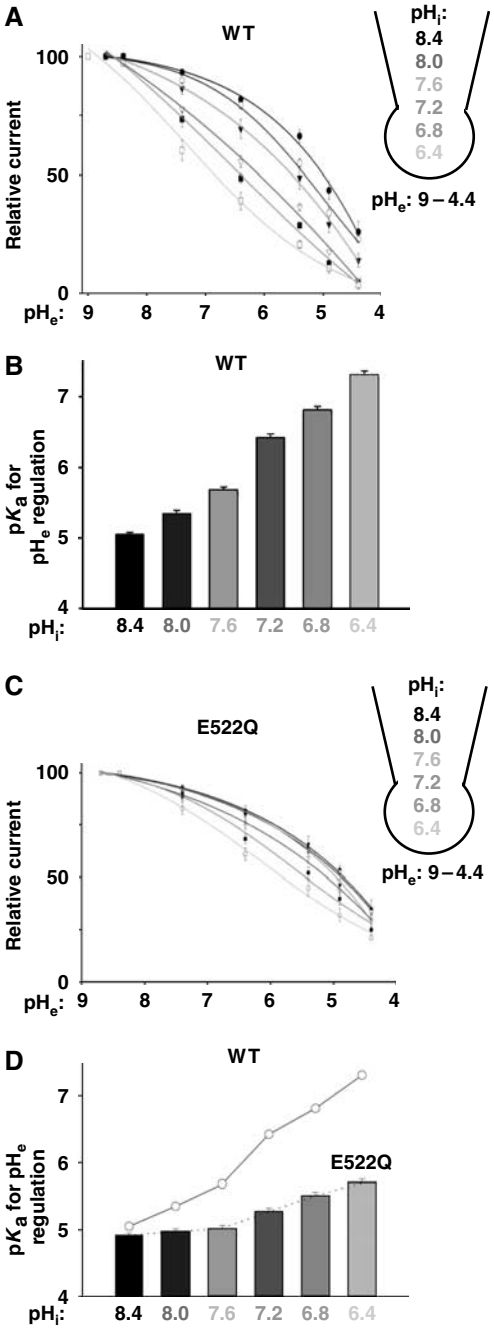

Figure 3 Modulation of pH_e regulation of TRPV5 by pH_i. (**A**) Dose–response curves for inhibition of WT TRPV5 by extracellular acidification (pH_e from 9.0 to 4.4) at different pH_i. Relative currents (normalized to the maximal current, labeled as 100) at any given pH_e are shown. (**B**) pK_a for pH_e regulation (*Y*-axis) at different pH_i (*X*-axis) for WT TRPV5. (**C**) Same as panel A, except for E522Q TRPV5 mutant. The mean inward current densities at pH_i 7.2 and pH_e 7.4 were 438 ± 29 pA/pF for E522Q mutant and 531 ± 42 pA/pF for WT. (**D**) Same as panel B, except for E522Q TRPV5 mutant. pK_a for WT (from panel B) is shown in circles connected by line for comparison.

acidification increases the sensitivity to extracellular protons. Glutamate-522 in the pre-pore helix region of TRPV5 is an pH_e sensor (Yeh *et al*, 2003). We found that modulation by pH_i or pH_e regulation was blunted in the E522Q mutant (Figure 3C and D), supporting that pH_i's and pH_e's cross-regulate the same gate.

Both intra- and extracellular acidification decrease the estimated diameter of TRPV5 pore

To investigate whether internal and external protons cross-regulate the selectivity filter gate, we first examined the effects of pH_i and pH_e on the estimated diameter of ion permeation pore. The pore diameter was estimated by measuring the relative permeability of organic monovalent cations of increasing size (Sabovcik *et al*, 1995; Voets *et al*, 2004).

Like many Ca^{2+}-permeating channels, TRPV5 conducts monovalent cations in the absence of Ca^{2+} ions (Nilius *et al*, 2001; Yeh *et al*, 2003). With Na^+ as the sole cation in the extra- and intracellular solution, TRPV5 currents reversed at 0 mV (-0.30 ± 0.52 mV, $n = 18$; Figure 4A). Replacing Na^+ in the extracellular solution with the same concentration of monomethylammonium (MA^+; 3.6 Å), dimethylammonium (DMA^+; 4.6 Å), or *N*-methyl-D-glucamine ($NMDG^+$; 6.8 Å) resulted in reductions of inward currents and shifts of reversal potentials toward negative membrane potentials. The permeability ratios of MA^+, DMA^+, and $NMDG^+$ relative to Na^+ (P_X/P_{Na}) were determined from the biionic reversal potential (Hille, 2001). The diameters (Å) of ion permeation pores were estimated (using a modified excluded volume

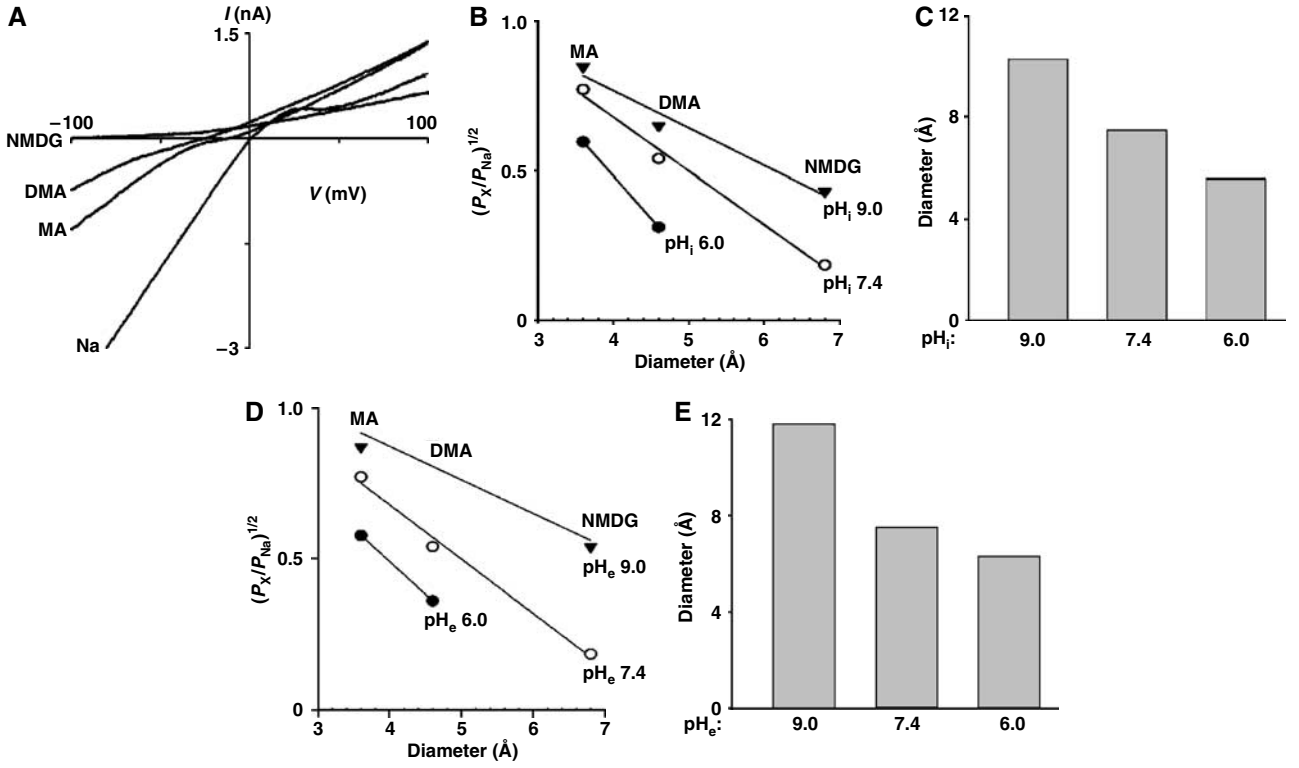

Figure 4 Effects of pH_i and pH_e on the estimated pore size. (**A**) Relative permeability of MA^+, DMA^+, and $NMDG^+$ to Na^+ at pH_i and pH_e 7.4. Whole-cell currents were first recorded in a bath solution containing 130 mM NaAsp, which was subsequently replaced by solutions containing 130 mM X-Asp. X is MA, DMA or NMDG. Shown are *I–V* curves at these different extracellular cations. The differential rectification in different extracellular cations and the reduction of outward currents in extracellular $NMDG^+$ may be due to pore block by partially permeant cations. (**B**) Relationships of the relative permeability ratios of permeating ions over Na^+ versus diameter of permeating ions at different pH_i's. Experiments were performed as in panel A, with pH_i at 9.0, 7.4, or 6.0. The relative permeability ratios (P_X/P_{Na}) were calculated according to the equation $P_X/P_{Na} = \exp \Delta E_{rev} \times F/RT$. ΔE_{rev} is the shift of reversal potential upon changing the bath solution from NaAsp to X-Asp. X is MA, DMA, or NMDG with diameters of 3.6, 4.6, and 6.8 Å, respectively. (**C**) Estimated pore diameter (Å) at pH_i's 9.0, 7.4, and 6.0. (**D**) Relationships of the relative permeability versus diameter of permeating ions at different pH_e's. (**E**) Estimated pore diameter at pH_e 9.0, 7.4, and 6.0.

equation $(P_X/P_{Na})^{1/2} = dP - dX/dP - dNa$, where dP, dX, and dNa are diameters of the pore, cation X^+, and Na^+, respectively; see Sabovcik *et al*, 1995) at ~10.3, 7.5, and 5.6 for pH_i's 9.0, 7.4, and 6.0, respectively (Figure 4B and C). These estimated pore diameter values agree with those using another excluded volume equation (Dwyer *et al*, 1980; Voets *et al*, 2004) (Supplementary Figure 3). Thus, intracellular acidification reduces the estimated TRPV5 pore diameter. Similarly, extracellular acidification reduces the estimated pore diameter. As shown in Figure 4D and E, the pore diameters (Å) were estimated at ~11.8, 7.5, and 6.3 for pH_e's 9.0, 7.4, and 6.0, respectively.

Effects of pH_i and pH_e on the monovalent cation selectivity of TRPV5

The effects of pH on the selectivity filter of TRPV5 were further investigated by examining the monovalent cation selectivity. Permeability ratios of Li^+, K^+, and Cs^+ relative to Na^+ were determined by replacing extracellular Na^+ with the respective ions. At pH_i 7.4, the relative permeability ratios of Li^+, K^+, and Cs^+ to Na^+ were 0.85 ± 0.04, 0.76 ± 0.04, and 0.65 ± 0.05, respectively (Figure 5A and Table I). This selectivity sequence ($Na^+ > Li^+ > K^+ > Cs^+$) follows Eisenman selectivity sequence X, indicating a strong-field-strength-binding site (Hille, 2001; Nilius *et al*, 2001). An increase in the diameter of the selectivity filter would decrease the electrostatic field strength of the ion-binding site. Indeed, we found that increasing pH_i from 7.4 to 9.0 changed the selectivity sequence to Eisenman III or IV, indicating a weak-field-strength-binding site (Figure 5B and Table I). These results support the idea that intracellular protons regulate the selectivity filter gate. Sequence X (at pH_i 7.4) represents the second strongest-field-strength-binding sequence among the 11 Eisenman sequences. Accordingly, decreasing pH_i from 7.4 to 6.0 did not change the Eisenman sequence (Table I).

We further examined the effects of pH_e on TRPV5 selectivity profile. Consistent with the results of increasing the pore diameter, extracellular alkalinization from pH 7.4 to 9.0 (at a fixed pH_i 7.4) altered the selectivity sequence from Eisenman sequence X to a weaker-field-strength-binding sequence (sequence IV or V; Table I). These results, together with the effects of pH on the pore diameter, indicate that both internal and external protons regulate the selectivity filter gate.

Intracellular acidification causes clockwise rotation of the pore helix

Amino acids 527–538 of TRPV5, likely from the pore helix of TRPV5 (Dodier *et al*, 2004; Voets *et al*, 2004), are similar to the pore helix of KcsA (Figure 6A). The selectivity filter of TRPV5 contains aspartate-542 critical for Ca^{2+} permeation (Nilius *et al*, 2001). The conformational state of pore helix is critical for the open conformation of selectivity filter (Doyle *et al*, 1998). We therefore hypothesized that internal and

external protons crossregulate the selectivity filter gate via conformational changes in the pore helix.

To test this hypothesis, we introduced cysteines into amino acids 529–537 of TRPV5 and examined reactivity of the mutants to extracellular membrane-impermeant cysteine-modifying reagent MTSET at either pH_i 8.4 or 6.8 (Figure 6B). Application of MTSET (1 mM) caused a fast inhibition of A529C at both pH_i's 6.8 and 8.4 (Figure 6C). The inhibition was not reversible by washout (not shown), indicating covalent modification of cysteine residues by MTSET. The second-order rate constants for inhibition were $\sim$200 and $\sim 75\,M^{-1}\,s^{-1}$ at pH_i's 6.8 and 8.4, respectively. In contrast, L530C was inhibited by MTSET at pH_i 8.4, but barely inhibited after 3 min application of MTSET at pH_i 6.8 (Figure 6D). F531C was not inhibited at either pH_i (Figure 6E); S532C was inhibited at pH_i 6.8, but not at pH_i 8.4 (Figure 6F). Figure 6G summarizes the effects of MTSET on cysteine-substituted amino acids from A529C to F537C. A529C, L530C, T533C, L536C, and F537 were >75% inhibited by MTSET at pH_i 8.4 in 3 min, whereas F531C, S532C, F534C, and E535C were not. As in helical wheel projection, amino acids sensitive to MTSET are located in the same face of the helix (Figure 6H). In contrast, the MTSET-resistant amino acids are located in a separate face. Assuming that lack of irreversible inhibition reflects inaccessibility to MTSET, these results indicate that the face of pore helix bound by L536 and L530 is exposed to solvents at pH_i 8.4. Interestingly, the solvent-exposed face at pH_i 6.8 is different from that at pH_i 8.4. As shown in Figure 6G and H, E535C and S532C were not accessible at pH_i 8.4, but accessible at pH_i 6.8. In contrast, F537C and L530C, two of the residues accessible at pH_i 8.4, were not accessible at pH_i 6.8 (Figure 6G and H). TRPV5 is mostly open at pH_i 8.4 ($\sim$90% of the maximal current) and predominantly closed at pH_i 6.8 ($\sim$30% of the maximal current). Thus, closing of TRPV5 by internal protons is associated with a clockwise rotation of the pore helix.

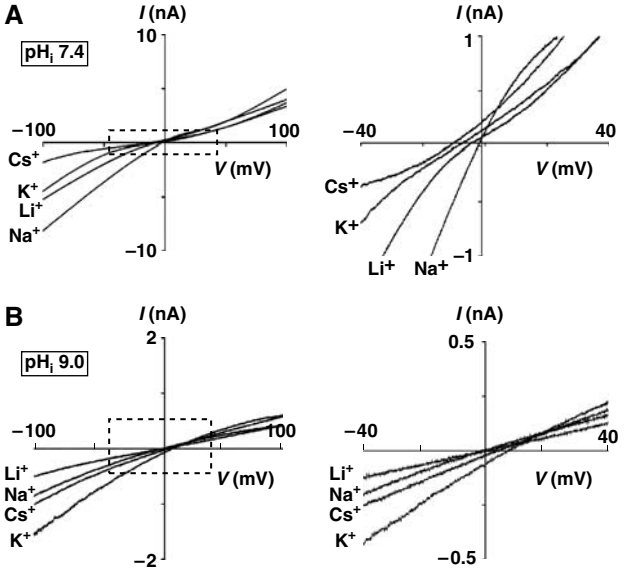

Figure 5 Relative permeability of inorganic monovalent cations to Na^+ at pH_i 7.4 (**A**) or 9.0 (**B**). Whole-cell experiments were performed with extracellular at pH 7.4 and pH_i at 7.4 (panel A) or 9.0 (panel B). Currents were first recorded in a bath solution containing 130 mM NaAsp, which was subsequently replaced by solutions containing 130 mM X-Asp. X is Li, Cs, or K. Shown are *I–V* curves at these different extracellular cations. The two left panels show *I–V* curves in the full range. The right panels show *I–V* curves of the boxed regions in an expanded scale.

Cysteine substitution of pore helix does not affect gating by protons

To exclude that cysteine substitution affects gating by protons, we examined three representative cysteine-substituted mutants (L530C, F531C, and S532C) located in separate faces of the pore helix (see Figure 6H). As shown in Figure 6, L530C is accessible at pH_i 8.4, but not at 6.8, whereas F531C is not accessible at either pH_i. S532C is accessible at pH_i 6.8, but not at 8.4. Here, we found that the sensitivity to pH_i for each of L530C, F531C, and S532C mutants was not different from that of wild-type (WT) TRPV5 (Figure 7A). Also, the sensitivity to pH_e and its modulation by pH_i for the mutants were essentially the same as for the WT (Figure 7B–F). These results indicate that cysteine substitution for L530, F531, and S532 does not affect gating by pH, and support our conclusion that changes in MTSET reactivity for amino acids in the pore helix are due to rotation along its along axis.

Amino acid aspartate-542 is important for intracellular acidification-induced changes of the pore diameter

Mutation of aspartate-542 of TRPV5 to alanine (D542A) increases the estimated pore diameter (Voets *et al*, 2004), suggesting that the side chain of aspartate-542 lines the narrowest part of the ion permeation pathway, forming the molecular sieve for permeating ions. We found that, unlike for WT TRPV5, the relative permeability of MA^+, DMA^+, and $NMDG^+$ to Na^+ for D542A mutant was not altered by intracellular acidification (Figure 8A; see Figure 4B for comparison). The estimated pore diameters (Å) at pH_i's 9.0, 7.4, and 6.0 for D542A mutant were $\sim$10, 9.7, and 9.2, respectively (Figure 8B). For comparison, the estimated pore diameter (Å) at pH_i's 9.0, 7.4, and 6.0 for WT TRPV5 were $\sim$10.3, 7.5, and 5.6, respectively (see Figure 4C). These results support the conclusion that intracellular protons regulate the selectivity gate of TRPV5 formed by aspartate-542.

Table I Effects of pH's on relative permeability of inorganic monovalent cations to Na^+

		K^+	Li^+	Cs^+	Permeability sequence	Eisenman sequence
pH_i (at fixed pH_e 7.4)	6.0	0.80±0.09	0.92±0.03	0.71±0.05	Na>Li>K>Cs	X
pH_i (at fixed pH_e 7.4)	7.4	0.76±0.04	0.85±0.04	0.65±0.05	Na>Li>K>Cs	X
pH_i (at fixed pH_e 7.4)	9.0	1.15±0.13	1.01±0.11	1.09±0.10	K>Cs>Na=Li	III or IV
pH_e (at fixed pH_i 7.4)	7.4	0.79±0.04	0.91±0.04	0.68±0.05	Na>Li>K>Cs	X
pH_e (at fixed pH_e 7.4)	9.0	1.10±0.07	0.88±0.11	0.98±0.11	K>Na=Cs>Li	IV or V

Data shown are the relative permeabilities of the respective ions to Na^+ (mean±s.e.m.).

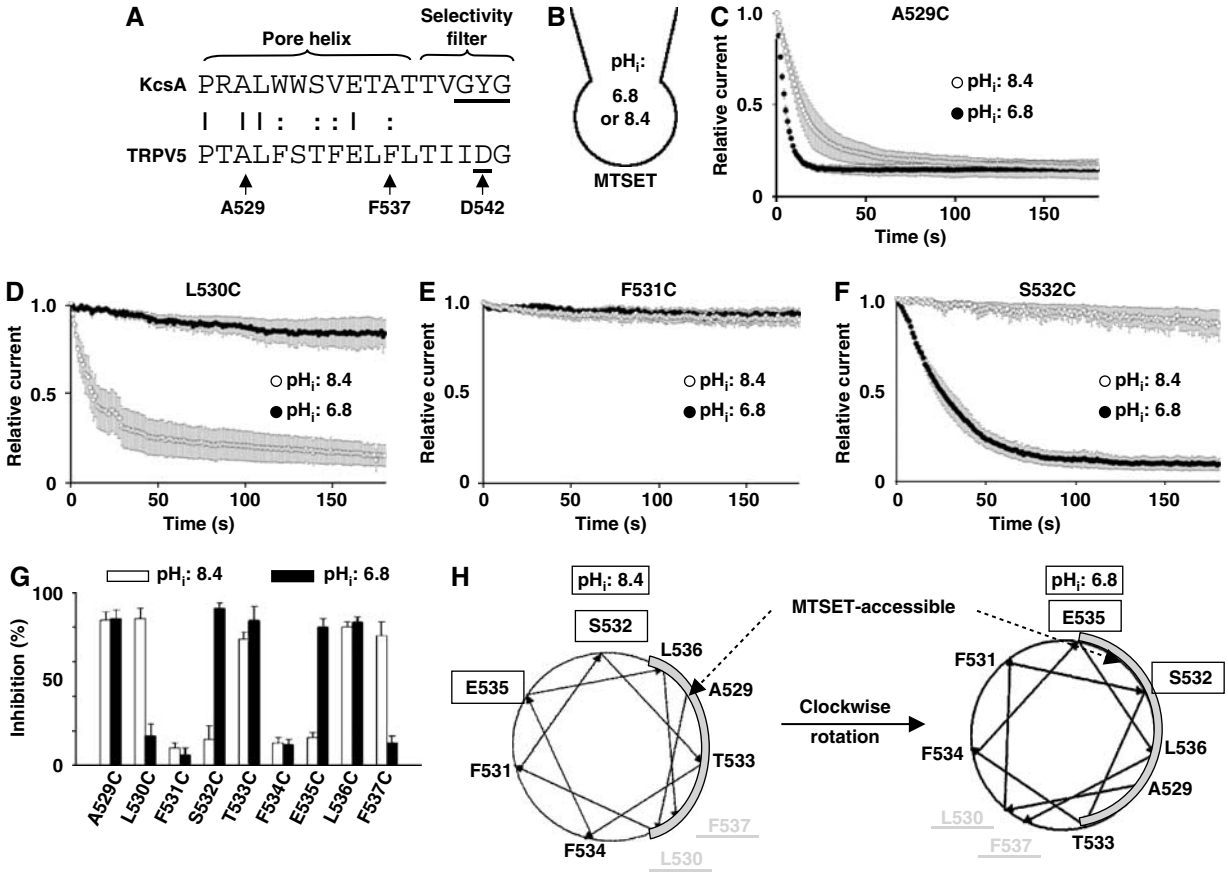

Figure 6 Accessibility of the pore helix to MTSET. (**A**) Alignment of the pore helix and selectivity filter of TRPV5 versus KcsA. Amino acids 527–543 of TRPV5 are shown. D542 of TRPV5 is critical for permeation of Ca^{2+} ions. Amino acids A529–F537 were individually mutated to cysteine. (**B**) Illustration of externally applied MTSET (1 mM) in whole-cell recordings at pH_i 8.4 or 6.8. (**C–F**) Effects of MTSET on A529C (C), L530C (D), F531C (E) or S532C (F) at pH_i 8.4 (○) or 6.8 (●). Inward currents (at −100 mV) from voltage ramp applied every second. Cells were transfected with varying amounts of DNA (0.5–5 μg) to produce similar current density for different mutants (ranging from 354±42 to 554±57 pA/pF at −100 mV and pH_e 8.4). Currents were normalized to the maximal current prior to application of MTSET. (**G**) Percent inhibition by MTSET (after 3 min) of cysteine-substituted mutants (from A529 to F537) at pH_i 8.4 (white bar) or 6.8 (black bar). (**H**) Helical wheel projection of amino acids of the pore helix of TRPV5. MTSET accessibility area of the pore helix is shown in gray. E535 and S532 are not accessible at pH_i 8.4, but become accessible at 6.8. In contrast, L530 and F537 are accessible at pH_i 8.4, but become inaccessible at 6.8. Amino acids L536, A529, and T533 are accessible at both pH_i's. Amino acids F531 and F534 are inaccessible at either pH_i.

The physiological function of TRPV5 is to mediate transepithelial Ca^{2+} transport. pH_e affects TRPV5-mediated Ca^{2+} entry (Yeh *et al*, 2003). Here, we further examined the effects of pH_i on Ca^{2+} permeation and selectivity. Whole-cell Na^+ current (at pH_i 9.0, 7.4, or 6.0) was first recorded in a bath solution containing (in mM) 140 NaAsp (Figure 8C). Subsequently, current was recorded in a bath containing (in mM) 130 NaAsp plus 10 $CaCl_2$. Owing to the anomalous mole fraction effect, inward currents would be predominantly carried by Ca^{2+} ions in the 10 mM $CaCl_2$-containing solution (Vennekens *et al*, 2001). The intracellular solution contains 140 mM Na^+. As shown in a representative recording at pH_i 7.4, currents reversed at ~0 mV in the 140 mM Na^+-containing bath solution, indicating Na^+ currents (Figure 8D; labeled 'Na^+'). In the 10 mM Ca^{2+}-containing bath solution, currents reversed at a positive membrane potential (indicated by the upward arrow), indicating inward Ca^{2+} currents (Figure 8D; labeled 'Ca^{2+}'). Ca^{2+} entry through TRPV5 raises the local intracellular Ca^{2+} concentration and causes feedback inhibition of the channel (Vennekens *et al*, 2000). As shown, TRPV5 Ca^{2+} currents decreased over 4 s (Figure 8D; labeled '1–4'). The magnitude of the first Ca^{2+} current (at −100 mV) recorded immediately after changing to the Ca^{2+} solution (labeled '1' in Figure 8D) was rather consistent (about 50–60% relative to that of the Na^+ current in all experiments) and thus used for examining effects of pH_i on TRPV5-mediated Ca^{2+} current. Similar to the Na^+ current (labeled 'Ina'), intracellular acidification and alkalinization decreased and increased Ca^{2+} current, respectively (labeled 'Ica'; Figure 8E). Thus, the regulation by pH_i is likely important for the physiological function of TRPV5 in Ca^{2+} transport.

The effect of pH_i on Ca^{2+} selectivity was examined by measuring the relative permeability ratio of Ca^{2+} to Na^+ (P_{Ca}/P_{Na}). As reported by others (Nilius *et al*, 2001), we found that TRPV5 was highly Ca^{2+}-selective and D542A mutation markedly decreased the selectivity (P_{Ca}/P_{Na} at pH_i 7.4: 65±7 and 3.2±0.4 for WT TRPV5 and D542A mutants, respectively; Figure 8F). Interestingly, the relative permeability ratio of Ca^{2+} to Na^+ was decreased by either alkalinization to pH_i 9.0 or acidification to pH_i 6.0 ($P<0.05$ versus pH_i 7.4; Figure 8F and Supplementary Figure 4). These results are consistent with the idea that the side chains of aspartate-542 of selectivity filter are oriented to provide the most stable interaction with Ca^{2+} ions at physiological pH_i ~7.4.

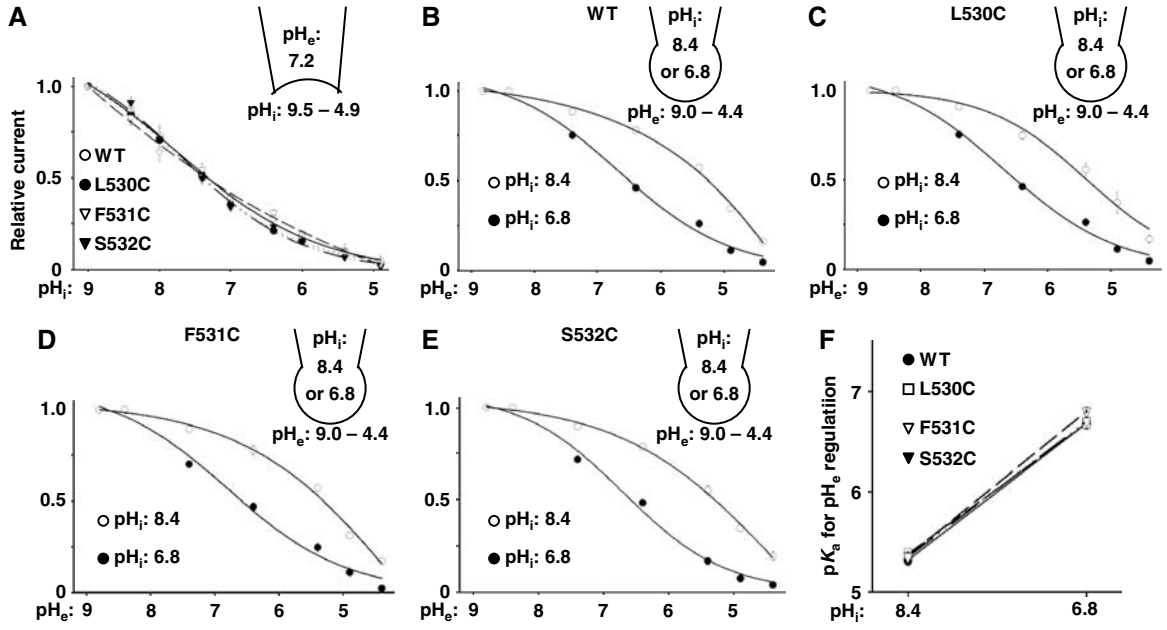

Figure 7 No effects of cysteine substitution on pH gating. (**A**) pH_i regulation of L530C, F531C, and S532C mutants versus WT. Relative currents (maximal current = 1) versus pH_i's are shown. (**B–E**) Dose–response curves for pH_e regulation at pH_i 8.4 or 6.8 for WT (B), L530C (C), F531C (D), and S532C (E). (**F**) pK_a for pH_e regulation at pH_i 8.4 and 6.8 for WT, L530C, F531C, and S532C. pK_a values are from panels B, C, D, and F, respectively.

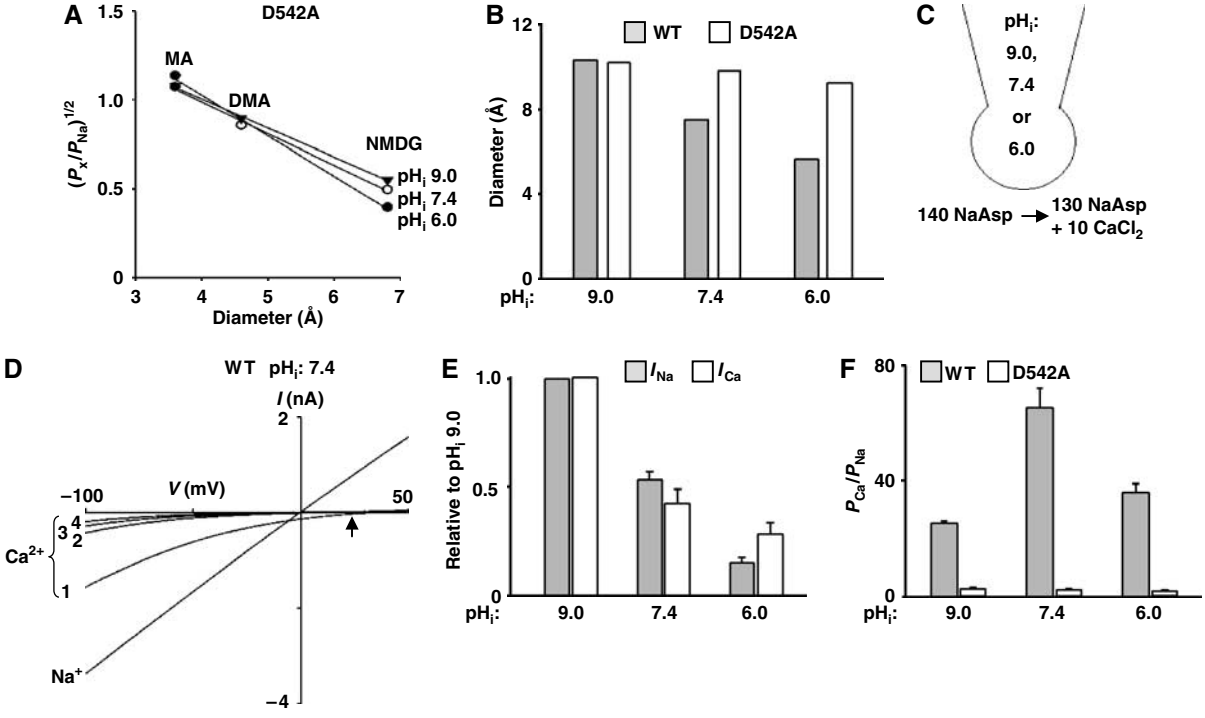

Figure 8 Role of aspartate-542 in pH_i-mediated changes of the pore diameter. (**A**) The relative permeability ratios of permeating ions over Na^+ versus diameter of permeating ions at different pH_i's for D542A mutant. Experimental paradigm is as in Figure 4B. (**B**) Estimated pore diameter (Å) at pH_i's 9.0, 7.4, and 6.0 for D542A mutant. Experimental paradigm is as in Figure 4C. (**C**) Solutions and diagram of whole-cell experiments of the relative permeability ratio of Ca^{2+} versus Na^+. (**D**) *I–V* curves of WT TRPV5 currents recorded at 140 mM NaAsp bath solution (labeled as Na^+) and upon changing to 130 mM NaAsp + 10 mM $CaCl_2$ (labeled as Ca^{2+}). Upward arrow indicates reversal potentials in 130 NaAsp + 10 $CaCl_2$-containing bath solution. Currents inactivated rapidly in four sweeps (numbered 1, 2, 3, and 4; one voltage ramp sweep per second). (**E**) Effects of intracellular acidification on Na^+ versus Ca^{2+} currents. Experimental paradigm is as shown in panels C and D. Na^+ currents ('Ina', gray bar) are inward currents (−80 mV) at 130 mM NaAsp-containing bath solution. Ca^{2+} currents ('Ica', white bar) are inward currents (at −80 mV) from the first sweep after changing to Ca^{2+}-containing bath solution. Currents at pH_i's 7.4 and 6.0 were normalized to pH_i 9.0. Mean ± s.e.m., $n = 12$–15 for each group. (**F**) Relative permeability ratio of Ca^{2+} versus Na^+ (P_{Ca}/P_{Na}) for WT TRPV5 (gray bar) and D542A mutant (white bar) at different pH_i's (9.0, 7.4, 6.0). The permeability ratio of Ca^{2+} versus Na^+ was calculated according to the equation, $P_{Ca}/P_{Na} = ([Na^+]_i/4[Ca^{2+}]_o)\exp(\Delta E_{rev}F/RT)\ \{(1+\exp(\Delta E_{rev}F/RT)\}$. ΔE_{rev}'s (shift of reversal potential from Na^+ to Ca^{2+} bath solution) were 7.6 ± 2.5, 22.3 ± 4.5, and 13.5 ± 2.2 mV for pH_i's 9.0, 7.4, and 6.0, respectively (see Supplementary Figure 4). Mean ± s.e.m., $n = 8$–12 for each group.

Displacement of the side chains caused by rotation of the pore helix (either clockwise rotation at pH_i 6.0 or counter-clockwise rotation at pH_i 9.0) destabilizes the interaction between side chains and Ca^{2+} ions and decreases the selectivity for Ca^{2+}. The decrease in the relative permeability of Ca^{2+} to Na^+ by intracellular acidification, together with the decrease in single-channel conductance and open probability, leads to reduction of calcium entry. Intracellular alkalinization, however, causes an increase in single-channel conductance and open probability besides its effect on the relative permeability of Ca^{2+} to Na^+. The net effect of alkalinization on TRPV5 is to increase the calcium entry (see Figure 8E above).

Amino acid lysine-607 is important for pH_i sensing and crossregulation by intra- and extracellular protons

We further searched for pH_i sensor(s). There are more than 140 titratable amino acids in the intracellular portion of TRPV5. We focused on 17 amino acids surrounding the putative intracellular entrance of the pore (i.e., from the fourth TM domain to the proximal C-terminus; see Figure 9A). These include lysine-484 in the intracellular loop between the fourth and fifth TM domains (IC loop; Figure 9A), aspartate-489 and arginine-492 in the fifth TM domain, glutamate-535 and aspartate-542 in the pore region, tyrosine-595 in the sixth TM domain, and aspartate-580, histidine-582, arginine-584, glutamate-588, aspartate-590, glutamate-591, and lysine-607 in the proximal carboxyl-terminus of the channel. We mutated each of these amino acids to a nontitratable amino acid and found that only mutation of lysine-607 to asparagine (K607N) decreased the sensitivity of the channel to inhibition by intracellular acidification. The pK_a for inhibition by intracellular acidification were 7.41 ± 0.15 and 6.17 ± 0.13 for WT TRPV5 and K607N mutant, respectively ($P<0.05$, $n=5$ each; Figure 9B). We further examined a role of lysine-607 in the crosstalk between pH_i and pH_e. As in Figure 7F, intracellular acidification from pH_i

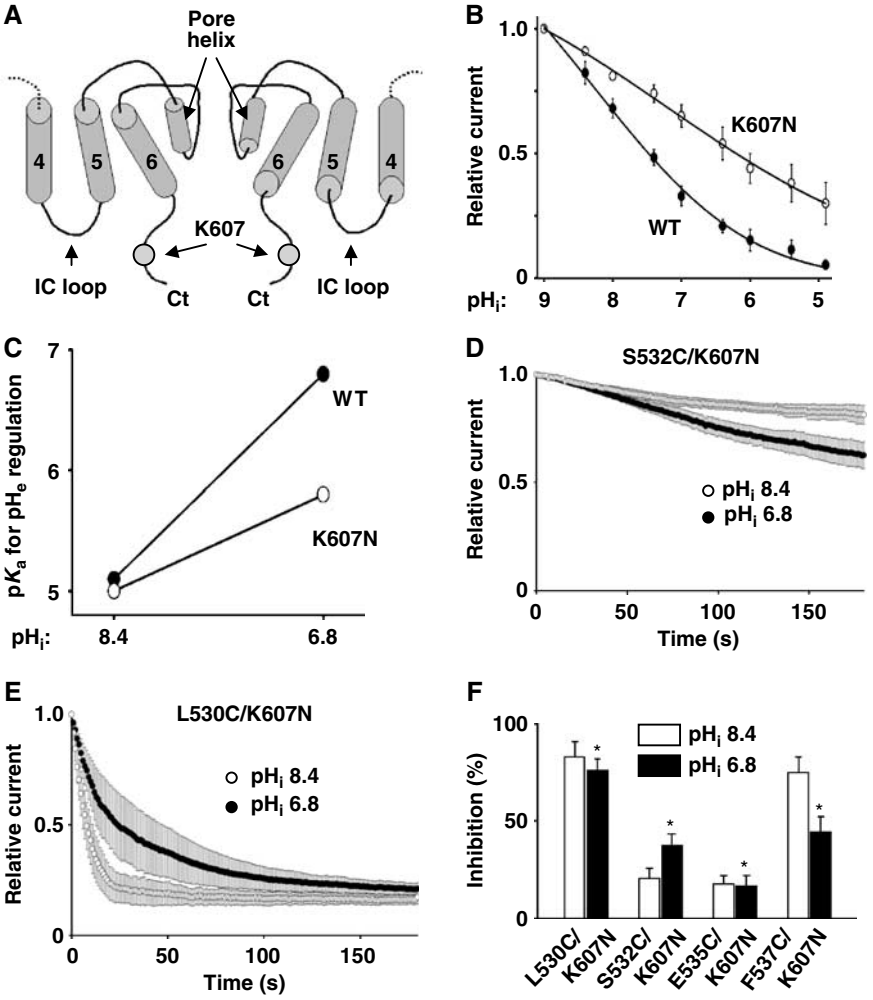

Figure 9 Amino acid lysine-607 is important for pH_i sensing and crossregulation by pH_i and pH_e. (**A**) Location of lysine-607 (K607) in the intracellular proximal carboxyl terminus (Ct). Illustrated is side-view of two subunits of a tetrameric channel. Only the fourth, fifth, and sixth TM (labeled '4', '5', and '6') and pore helices are shown. (**B**) Mutation of lysine-607 to asparagine (K607N) decreases intracellular acidification-mediated inhibition. Experimental paradigm is as in Figure 1. WT and K607N mutant channels in inside-out patches were exposed to pH_i ranging from pH 9 to 5. (**C**) pK_a for pH_e regulation at pH_i's 8.4 and 6.8 for WT (●) and K607N (○). Experimental paradigm is as in Figure 7F. pK_a's for pH_e regulation were studied using whole-cell recording at pH_i 8.4 or 6.8. (**D–E**) Effects of MTSET on double mutants S532C/K607N (D) and L530C/K607N (E) at pH_i 8.4 (○) or 6.8 (●). Experimental paradigm is as in Figure 6. (**F**) Percent inhibition by MTSET (after 3 min) of cysteine-substituted and K607N double mutants (L530C/K607N, S532C/K607N, E535C/K607N, and F537N/K607N) at pH_i 8.4 (white bar) or 6.8 (black bar). Experimental paradigm is as in Figure 6. * Indicates $P<0.05$ by unpaired *t*-test, double mutants versus single cysteine-substituted mutants at pH_i 6.8 taken from Figure 6G (L530C, S532C, E535C, and F537C, respectively).

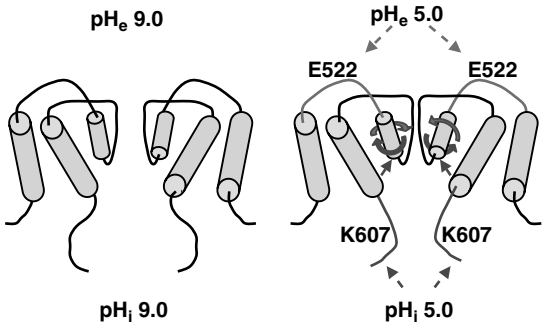

Figure 10 Model for crossregulation of TRPV5 by pH_i and pH_e. Conformational changes caused by intra- and extracellular acidification are illustrated. See text for details.

8.4 to 6.8 increased the pK_a for pH_e regulation of WT TRPV5 from 5.1 ± 0.07 to 6.8 ± 0.08 (Figure 9C). The increase in the pK_a for pH_e regulation by intracellular acidification was blunted for K607N mutant (pK_a: 4.9 ± 0.06 and 5.6 ± 0.06 at pH_i's 8.4 and 6.8, respectively). Thus, lysine-607 is an pH_i sensor that contributes to crossregulation by pH_i and pH_e.

S532C and E535C were not accessible to MTSET at pH_i 8.4, but accessible at pH_i 6.8. In contrast, L530C and F537C were accessible at pH_i 8.4, but not accessible at pH_i 6.8 (see Figure 6). These changes in accessibility are most consistent with the interpretation that intracellular acidification causes a clockwise rotation of the pore helix. We found that double mutants S532C/K607N (Figure 9D and F) and E535C/K607N (Figure 9F) were less sensitive to MTSET at pH_i 6.8 than single-cysteine mutants S532C and E535C, respectively (see Figure 6F and G). In contrast, double mutants L530C/K607N (Figure 9E and F) and F537C/K607N (Figure 9F) were more sensitive at pH_i 6.8 than single mutant L503C and F537C, respectively. Thus, K607 contributes to the rotation of pore helix associated with gating by internal protons. As controls, the effects of MTSET on double mutants at pH_i 8.4 (Figure 9D–F) were not significantly different from that on single mutants (Figure 6G). Also, the pK_a for pH_i regulation for the double mutants (6.21 ± 0.15, 6.09 ± 0.13, 6.26 ± 0.17, and 6.11 ± 0.14 for L530C/K607, S532C/K607N, E535C/K607N, and F537C/K607N, respectively; $n = 3$–4 for each) were not significantly different from that for K607N mutant (Figure 9B), confirming that cysteine substitution does not affect pH_i gating. These results support the conclusion that binding of protons to lysine-607 leads to rotation of the pore helix. Mutation of lysine-607 blunts the rotation caused by internal protons.

Discussion

Using the substituted cysteine accessibility method (SCAM), we report in this study that intracellular acidification causes conformational change(s) of the pore helix of TRPV5. One of the changes likely involves clockwise rotation of the pore helix along its long axis. This conclusion is based on the following assumptions. First, only cysteine residues at a water-accessible surface of the protein will react with MTSET. Second, reaction with MTSET will inhibit TRPV5. These two assumptions are likely valid in our present study given that MTSET is positively charged and membrane-impermeant (Holmgren *et al*, 1996) and that MTSET is large in size and the pore helix is in close proximity and critical for ion conduction (Doyle *et al*, 1998). Finally, intracellular acidification could, in theory, alter the local electrostatic environment of the cysteine residues and therefore affect their reactivity to MTSET without causing rotation of the pore helix (Wilson *et al*, 2000). However, the localization of MTSET-reactive and nonreactive residues to two separate, opposite faces of a predicted α-helix and the pattern of reactivity at pH_i 8.4 versus 6.8 (see Figure 6H) provide compelling evidence for a clockwise rotation of the pore helix caused by intracellular acidification. Other types of movements/conformational changes of the pore helix such as translation and/or tilting may also occur in intracellular acidification.

The pore helix of ion channels is critical for ion conduction. Aromatic amino acids of the pore helices of KcsA make contacts with aromatic amino acids in the selectivity filter to hold the filter open (Doyle *et al*, 1998). Moreover, pore helices point their carboxyl-termini to a water-filled cavity at the membrane center. The partial negative charge of the oriented pore helices provides a favorable electrostatic force to stabilize K^+ ions at the membrane center (Roux and MacKinnon, 1999). In the crystal structure of another bacterial K^+ channel KirBac1.1 in the closed state, pore helices no longer point directly at the center of the channel cavity (Kuo *et al*, 2003). It is believed that this misalignment of pore helices contributes to the closed state. For TRPV5, rotation with or without translation and/or tilting of the pore helix caused by intracellular acidification may cause a similar misalignment of the helix dipoles and close the channel. Rotation of the pore helix can also alter conformation of the selectivity filter.

Binding of extracellular protons to glutamate-522 in the pre-pore helix region of TRPV5 causes conformational changes and channel closure (Yeh *et al*, 2003). We find that pH_i modulates pK_a for pH_e regulation and *vice versa*. Mutation of glutamate-522 blunts the modulation by pH_i of pH_e regulation. Together, these results indicate that extra- and pH_i crossregulate the same activation gate. Where is this activation gate? The crystal structure of KcsA suggests two potential activation gates: an outer gate formed by the selectivity filter and pore helix and an inner gate formed by bundle crossing of four inner helices near the intracellular aspect of the membrane (Doyle *et al*, 1998; Flynn *et al*, 2001). Gating of voltage-dependent K^+ channels is associated with structural rearrangements of the inner helices and changes in their accessibility to intracellular Ag^+ (del Camino and Yellen, 2001), suggesting that bundle crossing is the activation gate in response to changes in TM voltage. Bundle crossing also serves as activation gate for intracellular signals. Phillips *et al* (2003) showed that gating of Kir6.2 channels by intracellular ATP involves movement of inner helices at the bundle crossing. Based on the crystal structure, Jiang *et al* (2002) proposed that opening of the MthK channel by intracellular Ca^{2+} occurs via bending of the inner helices at a hinge located deep in the membrane to splay open the bundle.

In contrast, studies of CNG channels revealed that, though the bundle crossing undergoes conformational changes associated with gating by intracellular cyclic nucleotide, it does not form a physical barrier for permeating ions in the closed state (Flynn and Zagotta, 2001). The pore helix and selectivity

filter of the CNG channels both undergo conformational changes in association with gating by intracellular cyclic nucleotide (Becchetti *et al*, 1999; Liu and Siegelbaum, 2000). Gating-associated movement of pore helix has also been found for other channels including voltage-dependent K^+ channels (Yang *et al*, 1997) and KcsA (Perozo *et al*, 1999). Whether the fifth and/or sixth TM helices of TRPV5 form an inner gate and, if so, whether they serve as an activation gate for internal protons is not known. Our results, nevertheless, suggest that the pore helix and selectivity filter of TRPV5 is at least one of the activation gates for intracellular protons (see the model in Figure 10). Gating by intracellular acidification occurs, at least partly, at the selectivity filter via rotation of the pore helix.

How does the pore helix senses intracellular protons? The inner helices of KcsA make direct contacts with pore helices (Doyle *et al*, 1998). It is believed that rotation of the pore helix of CNG channel in response to cGMP binding to the intracellular binding site occurs indirectly through conformational changes of the sixth TM inner helix (Flynn and Zagotta, 2001; Flynn *et al*, 2001). We propose that binding of protons to intracellular proton sensor(s) such as lysine-607 causes conformational changes of the sixth (and/or the fifth) TM helix (model in Figure 10). Conformational changes of the sixth TM helix then cause rotation of the pore helix of TRPV5 similarly to that in the CNG channel. Extracellular protons cause conformational changes of the channel by binding to a pH sensor (glutamate-522) located immediately upstream of the pore helix (Yeh *et al*, 2003). We suggest that both extra- and intracellular protons cause pore helices to rotate in the clockwise direction, leading to closing (narrowing) of the selectivity filter gate. Rotation of the pore helices by intracellular acidification will therefore facilitate closing of the channel by extracellular acidification and *vice versa*. This model of gating by protons at the level of pore helix and selectivity filter is supported by the results that protons decrease selectivity for Ca^{2+}, pore diameter, and the single-channel conductance, as well as reduction in open probability.

TRPV5 is the apical entry pathway for transepithelial Ca^{2+} transport in many tissues, including kidney, intestine, placenta, and prostate (Hoenderop *et al*, 2002). Overproduction of acid, as in metabolic acidosis or high dietary animal protein intake, inhibits renal transepithelial Ca^{2+} transport, causing increased urinary Ca^{2+} excretion and kidney stone diseases (Sutton *et al*, 1979; Huang, 2004). Most conditions of acid overproduction leading to kidney stone diseases cause both extra- and intracellular acidosis (such as high dietary animal protein intake) (Amanzadeh *et al*, 2003; Nicoletta and Schwartz, 2004). We report in this study that internal and external protons crossinhibit TRPV5-mediated Ca^{2+} entry. We suggest that inhibition of TRPV5-mediated renal Ca^{2+} transport by internal and/or external protons contribute to the pathogenesis of disturbances of Ca^{2+} transport in these diseases. Moreover, crossregulation by internal and external protons will allow the effects of extracellular acidosis on TRPV5 be modulated by the pH_i and *vice versa*. For example, extracellular acidification from pH_e 7.4 to 6.4 inhibits TRPV5 by 18% at pH_i 7.6, but by 24% at pH_i 6.8 (see Figure 3A). Thus, the combined effects of extra- and intracellular acidosis on calcium transport may be amplified or blunted depending on existing pH_e and pH_i.

Gating of ion channels in response to external and internal signals is a crucial cell function. How signals regulating ion channels are integrated across the cell membrane is poorly understood. The pore helix of ion channels is pivotal for ion conduction through the selectivity filter and accessible to both external and internal signals (Flynn *et al*, 2001). Thus, conformational changes of the pore helix may be a common mechanism for integrating extra- and intracellular signals in the regulation of ion channels.

Materials and methods

Molecular biology and cell culture

Mutant rabbit TRPV5's in pCDNA3 mammalian expression vector were constructed as described (Yeh *et al*, 2003). Chinese hamster ovary (CHO) cells (at ~50% confluence) were cotransfected with cDNA for pEGFP (0.5 μg) plus cDNAs for WT or mutant TRPV5 (0.5–5 μg) using lipofectamine-plus transfection kits (Gibco) as described (Yeh *et al*, 2003). About 24–48 h after transfection, cells were dissociated by limited trypsin treatment and placed in a chamber for recording. Transfected cells were identified using epifluorescent microscopy for recordings.

Electrophysiological recordings

Inside-out and whole-cell recordings were performed using an Axopatch 200B patch-clamp amplifier (Axon Instruments) (Yeh *et al*, 2003). For whole-cell recordings, the pipette and bath solution contained (in mM) 140 Na-Asp (sodium aspartate), 10 NaCl, 10 EDTA, 10 HEPES (titrated to pH as specified) and 140 Na-Asp, 10 NaCl, 1 EDTA, and 10 HEPES (pH as specified), respectively. For inside-out recordings, membrane patches were excised into a bath solution containing (in mM) 140 NaAsp, 10 NaCl, 10 EDTA, and 10 HEPES (pH as specified).

To determine the relative permeabilities of MA^+, DMA^+, and $NMDG^+$ to Na^+ in whole-cell recordings, the initial bath and pipette solution contain (in mM) 130 Na-Asp, 10 NaCl, 1 EDTA, 10 HEPES (pH as specified) and 130 Na-Asp, 10 NaCl, 10 EDTA, 10 HEPES (pH as specified), respectively. Na-Asp-containing bath solution was then replaced by one that contains 130 X-Asp, 10 X-Cl, 10 HEPES, and 1 EDTA (X is MA, DMA, or NMDG). X-Asp solutions were prepared by mixing methylamine (Fluka Chemika), dimethylamine (Aldrich), or NMDG (Sigma) (preweighted to a final concentration of 140 mM) with aspartic acid (preweighted to a final concentration 130 mM) and HCl (preweighted to a final concentration 10 mM) and adjusted pH using MA, DMA, or NMDG, respectively. For determination of the relative permeabilities of K^+, Li^+, and Cs^+ to Na^+, K-Asp, Li-Asp, and Cs-Asp solutions were prepared similarly.

To test the accessibility of substituted cysteines, MTSET (Toronto Research Chemicals) was added to the bath solution from 100 mM stocks. Stock solutions were prepared daily and kept at 4°C until use. Voltage protocols for each experiment were described in the individual figure. Currents were low-pass filtered at 1 kHz using an eight-pole Bessel filter, sampled every 0.1 ms (10 kHz) with Digidata-1300 interface and stored directly onto a computer hard disk using pCLAMP9 software. Data were transferred to compact discs for long-term storage.

Data analysis

To analyze the sensitivity of the channel to inhibition by extracellular or intracellular protons, relative currents at different pH values were fitted with modified *Hill* equation using the SigmaPlot program (Yeh *et al*, 2003). To calculate the apparent second-order rate constant for inhibition of channels by MTSET, time constant was obtained by fitting the time course of inhibition of channels by MTSET with a single exponential. Rate constant was calculated by dividing the reciprocal of the time constant by concentration of reagent (Yeh *et al*, 2003). The permeability ratios of different monovalent cations versus Na^+ were calculated based on the shifts of reversal potential (ΔE_{rev}) on exchanging the extracellular solutions, $P_X/P_{Na} = \exp(\Delta E_{rev} \times F/RT)$, where R, T, and F have the usual meaning (Hille, 2001). MA^+, DMA^+, and $NMDG^+$ (pK_a 9.25, 10.62, and 9.5, respectively) dissociate significantly at pH 9.0. Thus, concentrations of ionized MA^+, DMA^+, and $NMDG^+$

at pH 9.0 were calculated using the respective pK_a. P_X/P_{Na} was calculated as $\exp(\Delta E_{rev} \times F/RT) \times ([Na^+]/[\text{ionized } X^+])$. The permeability ratio of Ca^{2+} versus Na^+ was calculated according to the equation, $P_{Ca}/P_{Na} = ([Na^+]_i/4[Ca^{2+}]_o) \exp(\Delta E_{rev} F/RT)\{(1 + \exp(\Delta E_{rev} F/RT)\}$. The activity coefficients for Na^+ and Ca^{2+} were assumed 0.75 and 0.33, respectively. All potentials were corrected for liquid junction potentials. Liquid junction potentials were calculated and verified experimentally (Neher, 1992; Barry, 1994). The diameter of ion permeation pore was estimated by fitting P_X/P_{Na} versus diameter of permeating ions using a modified excluded volume equation: $(P_X/P_{Na})^{1/2} = dP - dX/dP - dNa$, where dP, dX, and dNa are diameters of the pore, cation X^+, and Na^+, respectively (Sabovcik *et al*, 1995). Data are shown as mean ± s.e.m. of the number of observations. Statistical comparison was made using unpaired Student's *t*-test.

Supplementary data

Supplementary data are available at *The EMBO Journal* Online.

Acknowledgements

We thank Dr Michel Baum for critical reading of the manuscript. This study is supported by NIH grants (DK-20543, DK-54368, DK-59530) and an EIA (0440019N) from AHA. CLH holds the Jacob Lemann Professorship in the Calcium Transport of University of Texas Southwestern Medical Center.

References

Amanzadeh J, Gitomer WL, Zerwekh JE, Preisig PA, Moe OW, Pak CY, Levi M (2003) Effect of high protein diet on stone-forming propensity and bone loss in rats. *Kidney Int* **64:** 2142–2149

Barry PH (1994) JP Calc, a software package for calculating liquid junction potential corrections in patch-clamp, intracellular, epithelial and bilayer measurements and for correcting junction potential measurement. *J Neurosci Methods* **51:** 107–116

Becchetti A, Gamel K, Torre V (1999) Cyclic nucleotide-gated channels. Pore topology studied through the accessibility of reporter cysteines. *J Gen Physiol* **114:** 377–392

Clapham DE (2003) TRP channels as cellular sensors. *Nature* **426:** 517–524

del Camino D, Yellen G (2001) Tight steric closure at the intracellular activation gate of a voltage-gated K(+) channel. *Neuron* **32:** 649–656

Dodier Y, Banderali U, Klein H, Topalak O, Dafi O, Simoes M, Bernatchez G, Sauve R, Parent L (2004) Outer pore topology of the ECaC-TRPV5 channel by cysteine scan mutagenesis. *J Biol Chem* **279:** 6853–6862

Doyle DA, Morais-Cabral J, Pfuetzner RA, Kuo A, Gulbis JM, Cohen SL, Chait BT, MacKinnon R (1998) The structure of the potassium channel: molecular basis of K^+ conduction and selectivity. *Science* **280:** 69–77

Dwyer TM, Adams DJ, Hille B (1980) The permeability of the endplate channel to organic cations in frog muscle. *J Gen Physiol* **75:** 469–492

Flynn GE, Johnson Jr JP, Zagotta WN (2001) Cyclic nucleotide-gated channels: shedding light on the opening of a channel pore. *Nat Rev Neurosci* **2:** 643–651

Flynn GE, Zagotta WN (2001) Conformational changes in S6 coupled to the opening of cyclic nucleotide-gated channels. *Neuron* **30:** 689–698

Hille B (2001) *Ion Channels of Excitable Membranes*. Sunderland, MA: Sinauer Associates

Hoenderop JG, Nilius B, Bindels RJ (2002) Molecular mechanism of active Ca^{2+} reabsorption in the distal nephron. *Annu Rev Physiol* **64:** 529–549

Hoenderop JG, Voets T, Hoefs S, Weidema F, Prenen J, Nilius B, Bindels RJ (2003) Homo- and heterotetrameric architecture of the epithelial Ca^{2+} channels TRPV5 and TRPV6. *EMBO J* **22:** 1–10

Holmgren M, Liu Y, Xu Y, Yellen G (1996) On the use of the thiol-modifying agents to determine channel topology. *Neuropharmacology* **7:** 797–804

Huang C-L (2004) The transient receptor potential superfamily of ion channels. *J Am Soc Nephrol* **15:** 1690–1699

Jiang Y, Lee A, Chen J, Cadene M, Chait BT, MacKinnon R (2002) The open pore conformation of potassium channels. *Nature* **417:** 523–526

Jordt SE, McKemy DD, Julius D (2003) Lessons from peppers and peppermint: the molecular logic of thermosensation. *Curr Opin Neurobiol* **13:** 487–492

Kuo A, Gulbis JM, Antcliff JF, Rahman T, Lowe ED, Zimmer J, Cuthbertson J, Ashcroft FM, Ezaki T, Doyle DA (2003) Crystal structure of the potassium channel KirBac1.1 in the closed state. *Science* **300:** 1922–1926

Liu J, Siegelbaum SA (2000) Change of pore helix conformational state upon opening of cyclic nucleotide-gated channels. *Neuron* **28:** 899–909

Montell C, Birnbaumer L, Flockerzi V, Bindels RJ, Bruford EA, Caterina MJ, Clapham DE, Harteneck C, Heller S, Julius D, Kojima I, Mori Y, Penner R, Prawitt D, Scharenberg AM, Schultz G, Shimizu N, Zhu MX (2002) A unified nomenclature for the superfamily of TRP cation channels. *Mol Cell* **92:** 229–231

Neher E (1992) Correction for liquid junction potentials in patch-clamp experiments. *Methods Enzymol* **207:** 123–131

Nicoletta JA, Schwartz GJ (2004) Distal renal tubular acidosis. *Curr Opin Pediatr* **16:** 194–198

Nilius B, Vennekens R, Prenen J, Hoenderop JG, Droogmans G, Bindels RJ (2001) The single pore residue Asp542 determines Ca^{2+} permeation and Mg^{2+} block of the epithelial Ca^{2+} channel. *J Biol Chem* **276:** 1020–1025

Perozo E, Cortes DM, Cuello LG (1999) Structural rearrangements underlying K^+-channel activation gate. *Science* **285:** 73–78

Phillips LR, Enkvetchakul D, Nichols CG (2003) Gating dependence of inner pore access in inward rectifier K^+ channels. *Neuron* **37:** 953–962

Roux B, MacKinnon R (1999) The cavity and pore helices in the KcsA K^+ channel: electrostatic stabilization of monovalent cations. *Science* **285:** 100–102

Sabovcik R, Li J, Kucera P, Prod'Hom B (1995) Permeation properties of a Ca^{2+}-blockable monovalent cation channel in the ectoderm of the chick embryo: pore size and multioccupancy probed with organic cations and Ca^{2+}. *J Gen Physiol* **106:** 149–174

Sutton RA, Wong NL, Dirks JH (1979) Effects of metabolic acidosis and alkalosis on sodium and calcium transport in the dog kidney. *Kidney Int* **15:** 520–533

Vennekens R, Hoenderop JG, Prenen J, Stuiver M, Willems PH, Droogmans G, Nilius B, Bindels RJ (2000) Permeation and gating properties of the novel epithelial Ca^{2+} channel. *J Biol Chem* **275:** 3963–3969

Vennekens R, Prenen J, Hoenderop JGJ, Bindels RJM, Droogmans G, Nilius B (2001) Pore properties and ionic block of the rabbit epithelial calcium channel expressed in HEK 293 cells. *J Physiol* **530:** 183–191

Voets T, Janssens A, Droogmans G, Nilius B (2004) Outer pore architecture of a Ca^{2+}-selective TRP channel. *J Biol Chem* **279:** 15223–15230

Voets T, Janssens A, Prenen J, Droogmans G, Nilius B (2003) Mg^{2+}-dependent gating and strong inward rectification of the cation channel TRPV6. *J Gen Physiol* **121:** 245–260

Wilson GG, Pascual JM, Brooijmans N, Murray D, Karlin A (2000) The intrinsic electrostatic potential and the intermediate ring of charge in the acetylcholine receptor channel. *J Gen Physiol* **115:** 93–106

Yang Y, Yan Y, Sigworth FJ (1997) How does the W434F mutation block current in Shaker potassium channels? *J Gen Physiol* **109:** 779–789

Yeh B-I, Sun T-J, Lee JZ, Chen H-H, Huang C-L (2003) Mechanism and molecular determinant for regulation of rabbit transient receptor potential type 5 (TRPV5) channel by extracellular pH. *J Biol Chem* **278:** 51044–21052

